Commun Nonlinear Sci Numer Simulat 152 (2026) 109216

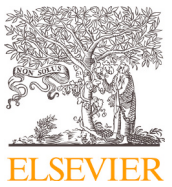

Contents lists available at ScienceDirect

Communications in Nonlinear Science and Numerical Simulation

journal homepage: www.elsevier.com/locate/cnsns

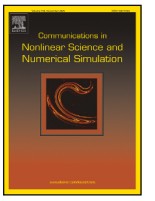

Cyclically symmetric Thomas oscillators as swarmalators: A model for active fluids and pattern formation

Vinesh Vijayan [a,*], Pranaya Pratik Das [b], K. Hariprasad [a], P. Satishkumar [a]

[a] Department of Science & Humanities, Rathinam Technical Campus, Coimbatore, Tamil Nadu, 641021, India
[b] Department of Physics and Astronomy, National Institute of Technology Rourkela, Rourkela, Odisha, 769008, India

ARTICLE INFO

Keywords:
Swarming
Collective motion
Pattern formation
Hexatic order
Turbulent motion

ABSTRACT

In this study, we demonstrate that cyclically symmetric Thomas oscillators can serve as swarmalators—agents exhibiting both swarming and phase synchronization—when coupled with Kuramoto-type phase dynamics. The resulting model represents a nonlinear particle aggregation system, characterised by cyclic spatial symmetry and position-dependent phase evolution. This coupling gives rise to rich spatio-temporal phenomena, including pre-hexatic or hexatic $2D$ structures, as well as chaotic turbulence under extreme parameter regimes. These emergent patterns result from nonl inear self-organization, manifesting as a form of active turbulence. Our analysis reveals that the nature and strength of inter-particle interactions, controlled by key system parameters, dictate the organization and dynamical behavior of the swarm. As a representative active, non-equilibrium system, this framework provides insights into the fundamental mechanisms of collective motion and offers applications in the design of synthetic active materials and coordinated microscale systems.

1. Introduction

Swarmalators have recently garnered significant attention in synchronization research, as they combine the spatial coordination of swarming with the temporal alignment of oscillators. These agents, modelled as mobile oscillators, differ from traditional examples like cardiac pacemakers or laser arrays by coupling spatial motion with internal phase dynamics [1,2]. Experimental studies show that local interactions and bidirectional coupling between position and phase are essential in governing their collective behavior, a principle applicable to bacterial populations with cyclically symmetric internal rhythms [3]. Like synchronization, swarming results from self-organization, where collective patterns emerge without centralised control. From a physics standpoint, swarmalators offer a unique lens into the properties of active matter, including energy distribution, dissipation, and self-propulsion, essential for understanding molecular motors and cellular motion.

Theoretical models continue to deepen our understanding of swarmalator dynamics, including nonlinear aggregation models with bounded inter-particle distances [4] and phase transitions in $2D$ systems of coupled oscillators [5]. Concepts like vision radius further clarify time-varying competitive phase interactions [6]. These findings are critical for decoding the behavior of self-propelled particles and micro-swimmers and offer promising pathways for developing responsive, programmable materials such as self-regulating soft robots [7]. Swarmalator models also aid in the design of active colloids—colloidal suspensions of interacting, self-driven agents capable of performing tasks autonomously [8–11].

* Corresponding author.
E-mail addresses: Vinesh.physics@rathinam.in (V. Vijayan), pranayapratik_das@nitrkl.ac.in (P.P. Das), hariprasad.maths@rathinam.in (K. Hariprasad), sathishkumarp.mech@rathinam.in (P. Satishkumar).

https://doi.org/10.1016/j.cnsns.2025.109216
Received 26 March 2025; Received in revised form 4 August 2025; Accepted 11 August 2025
Available online 14 August 2025

René Thomas introduced a simple yet rich model representing a particle within a $3D$ lattice, influenced by damping and external driving. The system,

$$\begin{aligned}\frac{dx}{dt} &= -bx + \sin(y),\\ \frac{dy}{dt} &= -by + \sin(z),\\ \frac{dz}{dt} &= -bz + \sin(x),\end{aligned} \tag{1}$$

features cyclic symmetry and a single control parameter b representing frictional damping. Its feedback structure enables transitions between regular and chaotic motion ([12–17]).

By integrating phase dynamics, this system transforms into a swarmalator, making it suitable for modelling active fluids. Such systems exhibit unique flow behaviors, including a turbulence-like regime where internal activity compensates for viscosity. This framework models the behavior of active colloids, where swarmalators operate in a damping medium, generating stress fields essential for understanding living matter [18,19]. These suspensions often contain micro- to nano-sized particles, whose macroscopic behavior depends on local interactions [20–22].

When particles propagate across a $3D$ lattice, the damping coefficient b regulates the collision frequency. Low b yields sparse collisions and near-conservative motion, while high b increases dissipation and suppresses motion. These dynamics produce complex, viscous flows, difficult to simulate with conventional techniques due to the deformable interfaces and multi-body interactions involved. The interplay between damping and inter-particle forces is central to modelling swarming behavior and understanding collective dynamics in active systems.

The remainder of this paper is organised as follows. Section 2 presents the general mathematical model of a swarmalator and its specific implementation using the Thomas system. Section 3 provides numerical results across varying damping and coupling regimes, revealing synchronization patterns and emergent structures. Section 4 discusses the implications of these findings, while Section 5 concludes with potential applications and future directions.

2. Mathematical modelling

2.1. The general framework and the swarming model

This work examines a realistic model of swarmalators moving freely in $3D$ space within a frictional environment. Swarming behavior arises through the coupling of spatial dynamics and internal phase dynamics. The general model is given by:

$$\begin{aligned}\frac{d\mathbf{r}_i}{dt} &= \mathbf{v}_i + \frac{1}{N}\sum_{j\neq i}^{N}[\mathbf{I}_A(\mathbf{r}_{ij})\mathcal{F}_A(\Theta_{ij}) - \mathbf{I}_R(\mathbf{r}_{ij})\mathcal{F}_R(\Theta_{ij})]\\ \frac{d\Theta_i}{dt} &= \omega_i + \frac{K}{N}\sum_{j\neq i}^{N}\mathcal{H}(\Theta_{ij})\mathcal{G}(\mathbf{r}_{ij})\end{aligned} \tag{2}$$

Here, $\mathbf{r}_{ij} = (r_j - r_i)$ is the inter-particle distance with $\mathbf{r}_i \in \mathbb{R}^3$ denotes the position, $\Theta_{ij} = \Theta_j - \Theta_i$ is the inter-particle phase difference with $\Theta_i \in S^1$ the phase, and ω_i the intrinsic frequency of the ith swarmalator. In swarming models, the phase is not merely an internal state of the oscillator but a critical factor governing its interactions with neighboring agents. The concept of phase similarity—where swarmalators attract or repel each other based on both their phase and spatial proximity—emphasizes the influence of this internal variable. The bidirectional coupling between phase and spatial dynamics gives rise to a variety of emergent collective states. The interaction terms $\mathbf{I}_A$, $\mathbf{I}_R$, $\mathcal{F}_A$, $\mathcal{F}_R$, $\mathcal{H}$, and $\mathcal{G}$ govern attraction, repulsion, and phase coupling.

For our specific model, we adopt the following form based on the Thomas oscillator:

$$\begin{aligned}\frac{d\mathbf{r}_i}{dt} &= \mathbf{f}(r_i) + \frac{1}{N}\sum_{j\neq i}^{N}\left[\frac{\mathbf{r}_{ij}}{r_{ij}}\Big(A + J\cos(\Theta_{ij})\Big) - B\frac{\mathbf{r}_{ij}}{r_{ij}^3}\right]\\ \frac{d\Theta_i}{dt} &= \frac{K}{N}\sum_{j\neq i}^{N}\frac{\sin(\Theta_{ij})}{r_{ij}^2}\end{aligned} \tag{3}$$

The spatial term $\mathbf{f}(r_i)$ follows the Thomas system dynamics (Eq. (1)), which includes an intrinsic damping parameter b. Eq. (3) reveals two competing spatial forces: short-range repulsion ($\propto 1/r_{ij}^3$) and long-range attraction modulated by the phase difference. We set $\mathcal{F}_R = 1$ and define $\mathcal{F}_A = A + J\cos(\Theta_{ij})$ to capture the influence of phase similarity on attraction. The phase coupling term varies with distance and is scaled by the interaction strength K.

By rescaling space and time, we fix $A = B = 1$. The sign and magnitude of J determine how phase similarity influences attraction: for $J > 0$, swarmalators with similar phases cluster; for $J < 0$, those with opposite phases cluster; and for $J = 0$, attraction is independent of phase. The parameter K controls phase synchronization: positive K promotes synchrony, while negative K promotes phase separation (Table 1) .

Table 1
Different swarming states. Static #(1–3) and dynamic #(4–5) swarming states.

#	Asymptotic State	Parameter Values	Abbreviation
1.	Static Sync	$J > 0,\ K = 1$	SS
2.	Static Async	$J > 0,\ K = -1$	SA
3.	Static Phase Wave	$J = 1,\ K = 0$	STPW
4.	Splintered Phase Wave	$J = 1,\ K \approx 0$	SPPW
5.	Active Phase Wave	$J = 1,\ K < 0$	APW

2.2. Characterization of swarming states

The spatial orientation of swarmalators and its correlation with phase play a crucial role in distinguishing between structured synchronous states—such as rotating clusters and phase waves—and asynchronous states, where phases are randomly distributed with respect to spatial position. The spatial orientation of the ith swarmalator is given by:

$$\Phi_i = \tan^{-1}\left(\frac{y_i}{x_i}\right) \tag{4}$$

To distinguish stationary from dynamic states, we define the mean velocity:

$$\mathcal{V} = \left\langle \frac{1}{N}\sum_{i=1}^{N}\sqrt{\dot{x}_i^2 + \dot{y}_i^2 + \dot{z}_i^2 + \dot{\Theta}_i^2}\right\rangle_t \tag{5}$$

where the angle brackets denote a time average. $\mathcal{V} = 0$ corresponds to static configurations, while $\mathcal{V} > 0$ indicates dynamic motion with time-varying phases.

The spatial spread of the swarm is quantified via the root-mean-square (r.m.s.) displacement:

$$D = \left\langle \sqrt{R^2}\right\rangle_t, \quad \text{where } R = \frac{1}{N}\sum_{j=1}^{N}\mathbf{r}_j \tag{6}$$

This measure reflects how mobility varies as a function of the damping parameter b in the Thomas oscillator.

3. Numerical experiments and observations

All swarmalators start in a cubic box with side length two, and their phases are initially drawn uniformly at random from $[\pi,\ -\pi]$. We then observe and analyse the subsequent collective dynamics.

At this point, we highlight the dynamics of an uncoupled Thomas oscillator. The dynamics are governed by the damping parameter b, which indicates the system's dissipative nature. Depending on b, we can tune the dynamics from fixed points at higher values to chaotic behavior at lower values ($b = 0$). The Lyapunov spectrum is shown in Fig. 1. For $b > 1$, the system has a single attractive fixed point $(0, 0, 0)$. Between $b = 1$ and $b = 0.328$, the system exhibits two attractive fixed points. At $b = 0.328$, the system undergoes a Hopf bifurcation, leading to the emergence of a limit cycle. When $b = 0.208$, the system transitions to chaotic behavior, with quasi-periodic windows appearing within the chaotic regime.

The term "damping" in the context of biology refers to the suppression of oscillations or fluctuations that helps stabilise the proper functioning of biological systems. This concept is closely linked to internal regulation mechanisms, such as feedback loops, as well as external influences. The Thomas system incorporates both of these elements.

3.1. Swarming states in the dissipative regime of Thomas oscillator.

3.1.1. Swarming states for $b > 1$

For $b > 1$, corresponding to high damping, the uncoupled Thomas oscillator has a single attractive equilibrium at $(x^* = y^* = z^* = 0)$. In this regime, swarmalators form a circularly symmetric, disk-like distribution in 3D space, centered at a fixed point and oriented. The $(x,\ y,\ z)$ coordinates are adjusted to highlight this planar symmetry. The characteristic disk radius emerges from the force balance between attraction and repulsion. Assuming phase synchrony, i.e., $\cos(\Delta\Theta) \approx 1$, from Eq. (7), this equilibrium condition implies,

$$\frac{A + J}{R_d} = \frac{B}{R_d^3} \tag{7}$$

$$R_d = \sqrt[2]{\frac{B}{A + J}} \tag{8}$$

For $A = 1,\ B = 1$ and for $J = 0.1$, the radium of the circular disk $R_d \approx 0.95$ matching the observation in the computational result Fig. 2.

From Eq. (7), we observe that as the value of J increases, the particles move closer together, leading to a shrinking of the cluster radius. This provides an estimate of the spatial extent of the cluster under phase synchronization conditions.

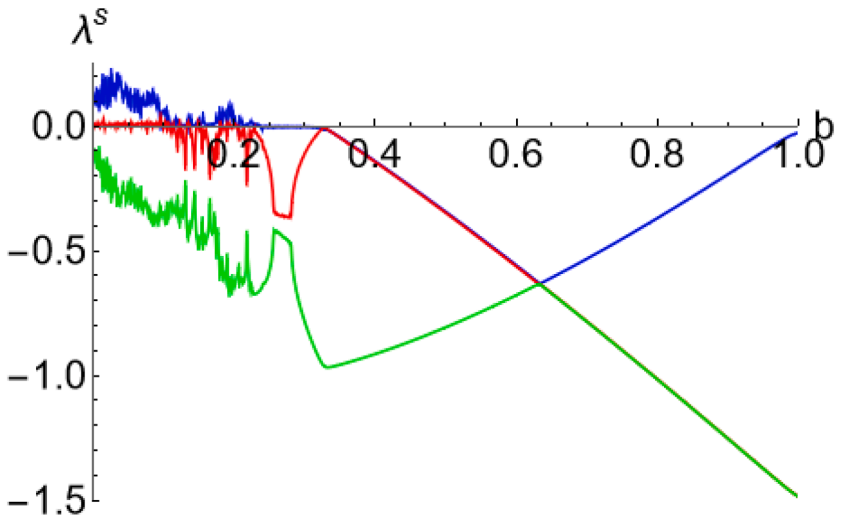

Fig. 1. Lyapunov exponents ($\lambda_1 \rightarrow$ blue, $\lambda_2 \rightarrow$ red, $\lambda_3 \rightarrow$ green) plotted against the damping parameter b. A chaotic regime is observed for $b < 0.208$, where $\lambda_1 > 0$. The exponents were computed using the Wolf algorithm with a time step $dt = 0.001$ and damping increment $\Delta b = 0.01$.

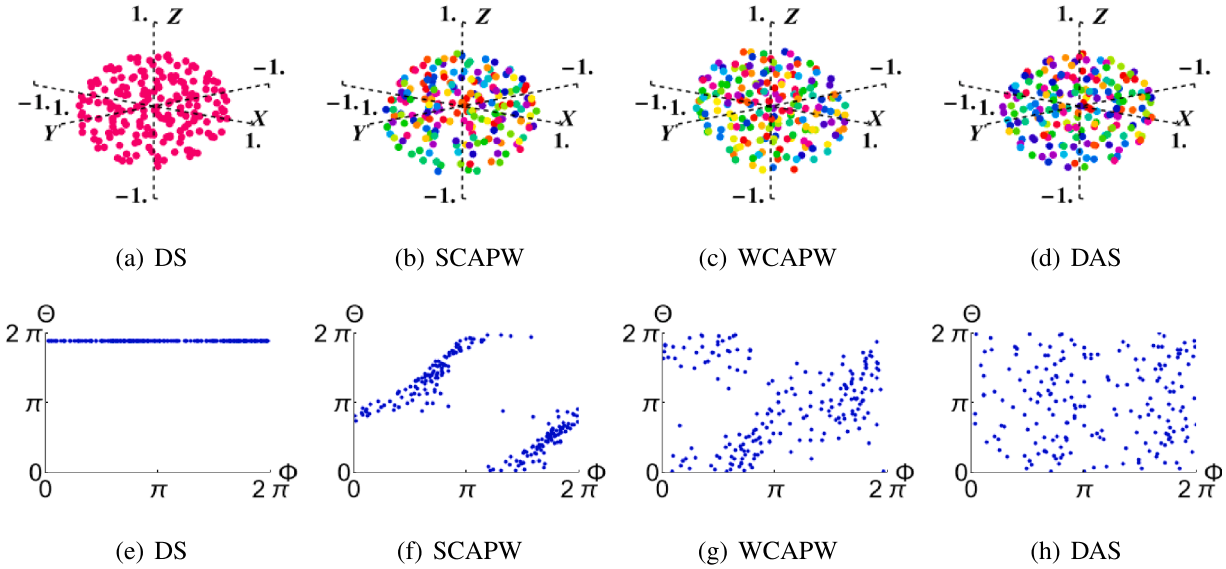

Fig. 2. **Top panel**: swarming states in $3D$ Space. **B**ottom panel: the $(\Phi,\ \Theta)$ distribution space for different swarming states. Simulations are done for $N = 200$ for $T = 1500$ time units with $dT = 0.01$ and $b = 1.2$. (a, e) DS $(J,\ K) = (0.\ 1,\ 1)$, (b, f) SCAPW $(J,\ K) = (1,\ 0)$, (c, g) WCAPW $(J,\ K) = (1,\ -0.3)$, (d, h) DAS $(J,\ K) = (0.1,\ -1)$. These are all circular disks formed in $3D$-Space.

At these higher damping values, static swarming states disappear. For instance, with $J > 0$ and $K = 1$, the system exhibits *Dynamic Synchronisation* (DS) (Fig. 2(a)), contrasting with the previously reported *Static Swarming* (SS) state [1]. Unlike SS, where particles remain spatially fixed and phases fully synchronise, in DS particles exhibit quivering motion within the disk, while their phases oscillate between two values, revealing bistability. This behavior points to the presence of multistability in the system (Fig. 3). This results in an intricate pattern resembling an irregular hexagonal structure, reflecting complex interactions.

After initial transients, the system reaches full phase synchronization, indicating coherence in internal states. The dynamic behavior stems from a balance between phase-dependent spatial interactions and damping, with continuous energy dissipation and replenishment. The non-zero mean velocity $\mathcal{V}$ $(= 0.8323)$ confirms this persistent activity, even though the disk as a whole remains stationary.

To study the intrinsic dynamical nature within the circular disc, we randomly selected a single oscillator for power spectrum analysis at two different values of the phase-dependent coupling strength J, keeping b fixed. At low coupling $J = 0.1$, the power spectrum (Fig. 4, left) shows broad peaks around four dominant frequencies, indicating chaos. For higher coupling $(J = 1)$, the spectrum (Fig. 4, right) narrows to two sharp peaks, reflecting more ordered yet complex dynamics. This transition also stabilises the oscillation amplitude, suggesting reduced chaos with increasing J.

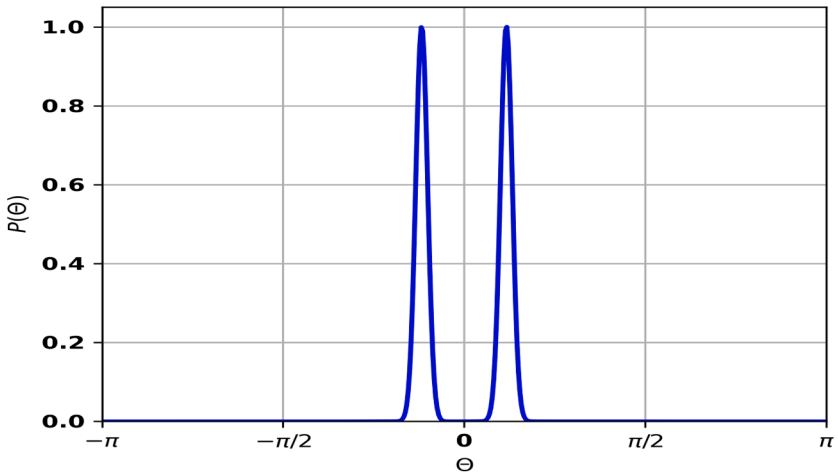

Fig. 3. The probability distribution for the phase in the DS state and shows bistability in phase dynamics. Two distinct states or modes of behavior depends on the initial conditions.

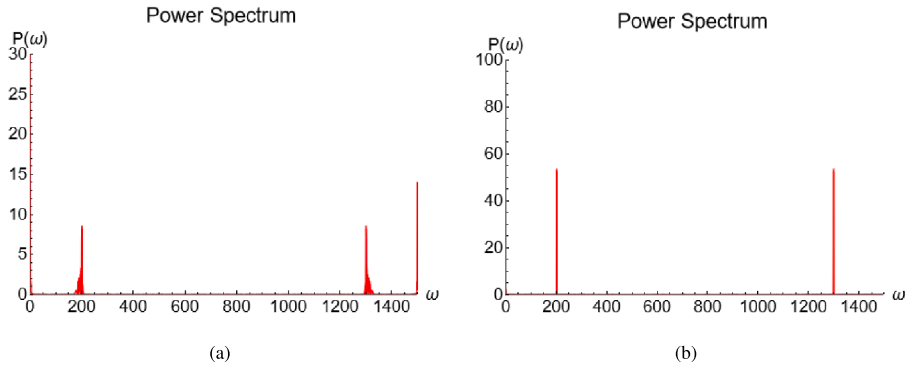

(a) (b)

Fig. 4. Power spectra of a randomly selected swarmalator from the circular disc. Simulations are done for $N = 200$ for $T = 1500$ time units with $dT = 0.01$ and $b = 1.2$. (a) $(J,\ K) = (0.1,\ high)$, (b) $(J,\ K) = (1,\ high)$. (a) stands for chaotic behaviour and (d) stands for quasi-periodic behaviour.

As the phase coupling strength K decreases from positive to negative values, the system transitions through several distinct dynamical states. For $K = 0$, where spatial-phase correlation is maximal, the system exhibits a *Strongly Correlated Active Phase Wave* (SCAPW) state. Here, swarmalators retain their initial phases, and due to $J = 1$, attempt to cluster based on phase similarity. However, strong damping ($b > 1$) suppresses full rearrangement, resulting in quivering motion within a circular disc, combining translational and rotational dynamics—thus forming an *Active Phase Wave* (APW). As K decreases slightly below zero, the amplitude of these oscillations increases, and swarmalators begin to move radially while maintaining periodic motion in both space and phase—leading to a *Weakly Correlated APW* (WCAPW).

With further reduction in K, the system enters a *Dynamic Asynchronous State* (DAS), characterised by spatially distributed swarmalators exhibiting a full range of phase values. Despite persistent motion ($\mathcal{V} \neq 0$), phase values are uniformly spread across space, reflecting a loss of phase-space correlation. The swarming transitions thus follow:

$$\text{DS} \longrightarrow \text{SCAPW} \longrightarrow \text{WCAPW} \longrightarrow \text{DAS}.$$

These transitions are visualized in Fig. 2 (top), with corresponding $(\Phi,\ \Theta)$ phase-space distributions shown in the bottom panel. In the DS regime (Fig. 2(e)), swarmalators synchronise to the same phase regardless of spatial orientation. In contrast, the DAS state (Fig. 2(h)) exhibits a uniform phase distribution across all spatial locations, indicating complete desynchronization. Intermediate APW states (Figs. 2(f)and (g)) show varying degrees of spatial-phase correlation that weaken as K becomes more negative.

Importantly, for $b > 1$, the system does not support *Static Phase Wave* (STPW) or *Static Phase Pulse Wave* (SPPW) states, even at $K = 0$ o r slightly negative K. The damping parameter b effectively opposes the attractive coupling J, suppressing static structures and favouring dynamic motion. This persistent activity mirrors behaviors observed in biological swarms, where continual movement arises from competing local and global interactions.

To understand the exact pattern within the circular symmetry, we calculated the *Hexatic Order Parameter* (HOP) [23] by projecting the system onto the intrinsic plane of the circular disc using *Principal Component Analysis* (PCA) [24] (see Supplementary Section 2). In $2D$ systems, the HOP serves as a critical tool to characterize positional and orientational order. Locally, the HOP quantifies how

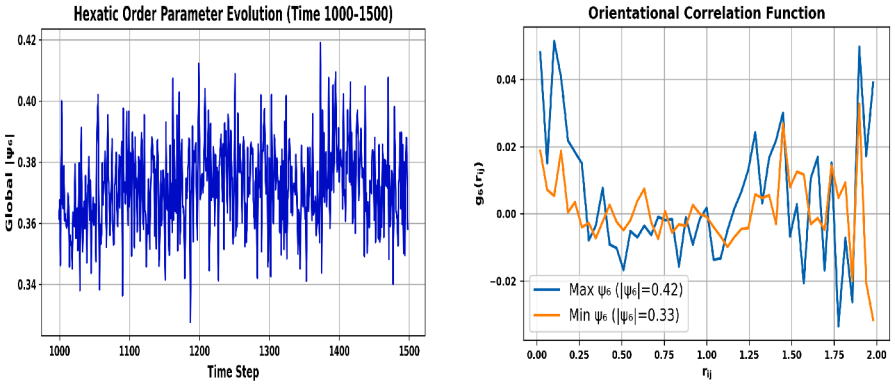

(a) (b)

Fig. 5. (a)The HOP calculated for the asymptotic states. The plot shows co-existence of hexatic and isotropic liquid-like states. This calculation is done for the DS state with $b = 1.2,\ J = 0.1,\ \&\ K = 1$ using Eq. (10)(b). The orientational co-relation function calculated for the maximum and minimum values of HOP. For both cases it exponentially decays, underlying short-range orientational order.

well the local arrangement of particles resembles a perfect hexagonal lattice, and it is defined as

$$\psi_6^i = \frac{1}{N_i}\sum_{j=1}^{N_i} e^{i6\theta_{ij}} \tag{9}$$

where $N_i =$ number of neighbours of particle i, the factor 6, a reflection of the 6-fold symmetry, plays a crucial role. The phase tells us the orientational structure of the bond network. This complex number $\psi_6(\mathbf{r}_i)$ measures how well the local neighbourhood resembles a perfect hexagonal arrangement. To assess the overall orientational order in the entire system of N particles, the global HOP is obtained by averaging the local parameters:

$$|\Psi_6| = \frac{1}{N}\sum_{j=1}^{N} \psi_6^i \tag{10}$$

To capture the system's steady-state behavior or long-term properties, this quantity is often further averaged over time.

$$\langle|\Psi_6|\rangle_t = \langle\frac{1}{N}\sum_{j=1}^{N} \psi_6^i\rangle_t \tag{11}$$

This two-step averaging—spatial and temporal—provides a robust and precise measure of the system's global orientational order. The magnitude of HOP for both the cases ranges from 0 (no hexagonal order or orientational order) to 1 (perfect hexagonal symmetry). And an intermediate value means a hexatic state where there is no long-range hexagonal order.

The time-averaged hexatic order parameter, $|\Psi_s| = 0.37$, lies above the commonly cited threshold (~ 0.30) that separates isotropic or pre-hexatic behavior from the onset of hexatic ordering [25,26]. Instantaneous values fluctuate between 0.33 and 0.42, indicating that the system intermittently enters a hexatic-like state before relaxing back toward isotropic configurations. This dynamic suggests the presence of transient, localized hexatic domains embedded within an otherwise disordered, liquid-like structure.

We calculated the orientational correlation function $g_6(r_{ij})$ for both high and low values of the *Local Hexatic Order Parameter* (LHOP) using a specific analytical expression:

$$g_6(r) = \langle\psi_6^i(r_i)\psi_6^j(r_j)\rangle_{r_{ij}} \tag{12}$$

This result is shown in Fig. 5(b). At steps 1373 and 1187, the LHOP reaches its maximum ($|\Psi_6| = 0.42$) and minimum ($|\Psi_6| = 0.33$), respectively. In both cases, $g_6(r)$ is positive at short range, indicating local orientational alignment. At intermediate ranges, $g_6(r)$ exhibits sign changes, reflecting oppositely oriented domains and the formation of competing patches. The resulting oscillations for higher values of r_{ij} suggest frustration and structural defects within the system, limiting global orientational order.

3.1.2. Swarming states for $b \in (0.328, 1)$

At $b = 1$, the uncoupled Thomas oscillator undergoes a pitchfork bifurcation, generating two symmetric attractive fixed points at$(x^* = y^* = z^* = \pm\sqrt{6(1-b)})$. For $b = 0.5$, swarmalators self-organise into clusters around these fixed points, forming mirror-symmetric disc-like distributions. These configurations resemble Zindler-type curves [see Supplementary Section 2], characterised by constant-density distributions akin to neutrally buoyant bodies in fluid.

Numerical simulations with 200 swarmalators show that depending on the interaction strengths, the system stabilises around either the positive or negative fixed point, preserving the same Zindler-type symmetry in each case, as illustrated in Fig. 6.

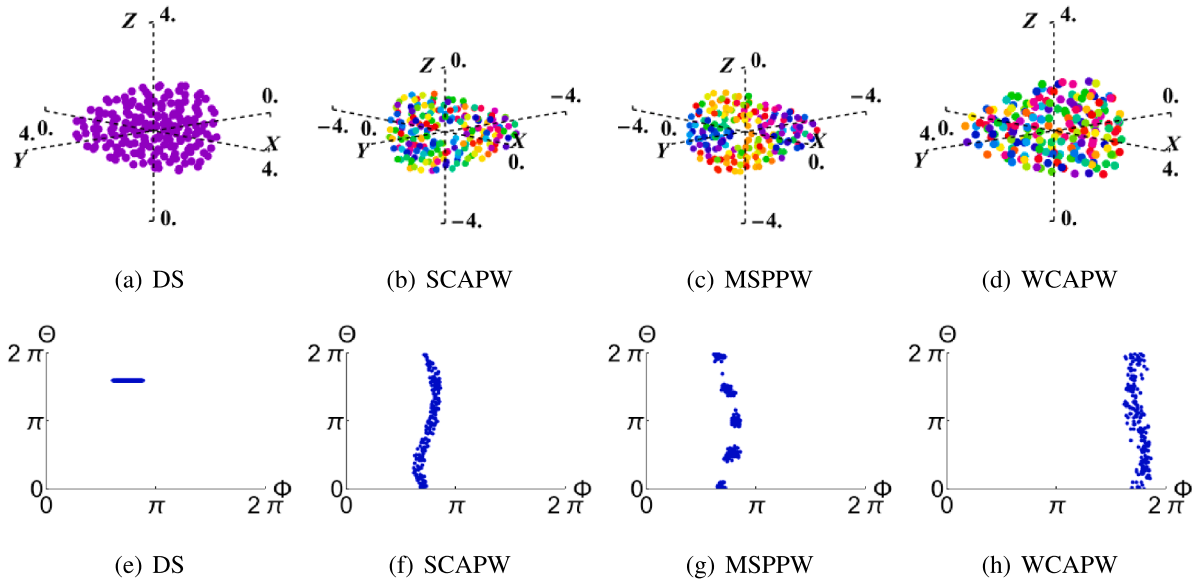

Fig. 6. **T**op panel: swarming states in $3D$ Space. **B**ottom panel: the $(\Phi,\ \Theta)$ distribution space for different swarming states. Simulations are done for $N = 200$ for $T = 1500$ time units with $dT = 0.01$ and $b = 0.5$. For all these steady states $\mathcal{V} \approx 0.9621$. (a, e) DS $(J,\ K) = (0.1,\ 1)$, (b, f) SCAPW $(J,\ K) = (1,\ 0)$, (c, g) MSPPW $(J,\ K) = (1,\ -0.03)$, (d, h) WCAPW $(J, K) = (1, -0.3)$.

For $K = 1$ and $J > 1$, the system displays a *Dynamic Synchrony* (DS) state characterised by irregular hexagonal lattices. As K decreases toward negative values, the system transitions through distinct states: *Strongly Correlated Active Phase Wave* (SCAPW) at $K = 0$ and $J = 1$, followed by a *Mixed Static Phase Pulse Wave* (MSPPW). Unlike the SPPW reported in [1], MSPPW features neighbouring phases within clusters rather than uniform phase synchrony. Further reduction in K leads to a *Weakly Correlated Active Phase Wave* (WCAPW). Here, reduced damping enhances the effect of J, reinforcing phase-dependent interactions. This progression of swarming states follows: $(DS \rightarrow SCAPW \rightarrow MSPPW \rightarrow WCAPW)$, as visualized in Fig. 6.

Analysis of $(\Theta,\ \Phi)$ distributions reveals that in DS, all particles share the same phase. In SCAPW, MSPPW, and WCAPW, particles explore the full phase range while remaining confined to narrow Φ regions, indicating directional movement. For $K = -1$ and $J > 0$, the disc centers around -1.73, likely representing a stable configuration. However, persistent phase-space correlations confirm WCAPW, not DAS. The distinction hinges on whether phase and spatial orientation remain correlated (APW-type) or decouple entirely (DAS). We calculated the hexatic order parameter, which exhibits behavior similar to the previous case, while the DS state displays clear phase bistability.

A new swarming state emerges for slightly positive values of K, with $j = 1, b = 0.5$ which we term *Phase Asymmetric Dynamic-Cluster Synchrony* (PADCS). In this state, the two clusters with spatial chiral orientation but have different phases. The swarmalators within each cluster achieve complete phase synchrony; however, the two clusters differ asymptotically in phase, resulting in a persistent phase asymmetry and phase symmetry is broken. This may be due to weaker phase coupling and stronger dissipation. Slight positive value of K promote localised phase synchrony and prevent global phase coherence facilitating asymmetric phase locking. Here also we find intermittent co-existence of hexatic/isotropic liguid-like behavior. The number of swarmalators in each cluster is sensitive to the value of K, indicating a delicate balance in the system's dynamics. This sensitivity highlights the complex nature of the phenomenon and suggests a need for further investigation. The clusters and their corresponding phase-space correlations are illustrated in Fig. 7.

Thus the observed *Non-Equilibrium Steady State* (NESS) represents a distinct concept that does not conform to the traditional notion of a well-defined thermodynamic phase. Instead, it fluctuates between exhibiting partial orientational order and a fully disordered state, indicating the absence of a sharp phase transition. Unlike equilibrium systems, which undergo phase transitions at well-defined critical points, the behavior of NESS reflects a fragile and dynamic balance between order and disorder, driven by continuous particle interactions and fluctuations. The origin of phase bistability stems from this intermittence co-existence of hexatic/isotropic liquid-like behaviour. This highlights the inherently non-equilibrium nature of the system, where structural organization is transient and emergent rather than fixed.

3.2. *Swarming states for* $b \in (0.0, 0.328]$

This section explores the dynamically rich domain of moderate damping parameter values, focusing specifically on $b = 0.3$ and $b = 0.1$. These values are chosen because $b = 0.3$ lies within the limit-cycle regime of the uncoupled Thomas oscillator, while $b = 0.1$ corresponds to a well-defined chaotic regime [see Fig. 1]. For this analysis, we fix the parameters to ensure complete phase synchronization $(J > 0,\ K = 1)$.

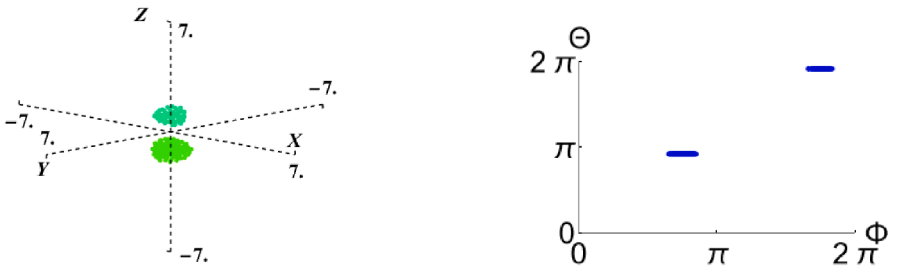

(a) PDCS (b) (Φ, Θ) Distribution

Fig. 7. (a) *Dynamic cluster synchrony* (PDCS), and (b) the corresponding (Φ, Θ) phase-space distribution. Simulations are performed with $N = 200$ over $T = 1500$ time units, using $dT = 0.01$ and $b = 0.5$. DCS occurs at $(J,\ K) = (1,\ \approx 0^{+})$.

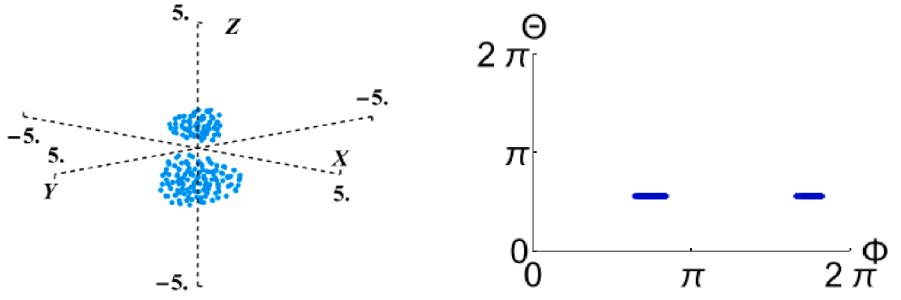

(a) $t = 1300$ (b) $t = 1300$

Fig. 8. (a) *Dynamic cluster synchrony* (DCS), and (b) the corresponding (Φ, Θ) phase-space distribution. Simulations are performed with $N = 200$ over $T = 1500$ time units, using $dT = 0.01$ and $b = 0.3$. DCS occurs at $(J, K) = (0.3, 1)$.

At $b = 0.3$ and $J = 0.3$, where the two interaction strengths are balanced, the swarmalators divide into two clusters. Each cluster evolves into a disc-shaped structure exhibiting Zindler curve symmetry and eventually settle into a dynamic cluster synchronised state (DCS). This is an important dynamic regime where the spatial chiral symmetry is broken as in the case of $PDCS$. When the value of J is increased or decreased from this balanced point, particles migrate between the clusters, eventually coalescing into a single cluster that manifests the dynamically synchronised state (DS). The two-cluster scenario exhibits phase symmetry, as illustrated in Fig. 8 and this symmetry likely results from the balance between the competing interaction strengths.

To examine the intrinsic dynamics in the limit cycle regime, we used PCA to project the clusters onto their intrinsic plane and computed the center of mass. In this plane, each particle's angular momentum relative to the COM was calculated using the $2D$ cross product of its position and velocity vectors.

$$\ell_i = \tilde{\mathbf{r}}_i \times \tilde{\mathbf{v}}_i = \tilde{r}_{i,x}\tilde{v}_{i,y} - \tilde{r}_{i,y}\tilde{v}_{i,x}, \tag{13}$$

Here, $\tilde{\mathbf{r}}_i$ and $\tilde{\mathbf{v}}_i$ are the projected position and velocity vectors of the ith particle in the PCA plane, and ℓ_i is the scalar out-of-plane angular momentum. The total and average angular momentum are then computed over all particles in the cluster.

$$L_{\text{total}} = \sum_{i=1}^{N} \ell_i, \quad \tilde{L} = \frac{1}{N}\sum_{i=1}^{N} \ell_i, \tag{14}$$

Here, N is the number of particles in the cluster, and ℓ_i is the angular momentum of the ith particle relative to the cluster's *Center of Mass* (CoM) in the projected plane. A positive $\tilde{L}$ indicates net counter clockwise rotation, while a negative value implies clockwise rotation.

Fig. 9 shows that Cluster 1, comprising 123 particles, exhibits a clear rotational structure. The velocity vectors, shown as blue arrows, form coherent circular patterns around the center of mass (red marker), indicating a dominant clockwise rotation. This is quantitatively supported by a total angular momentum of $L_{\text{total}} = -12.47041$ and an average angular momentum of $\tilde{L} = -0.09819$ in the PCA-defined plane. In contrast, Cluster 2, consisting of 67 particles, displays a more disordered structure. Its velocity vectors are scattered and largely cancel out, suggesting counter-rotating flows that effectively neutralize the net angular momentum. As a result, the total angular momentum is $L_{\text{total}} = -0.0125$ and the average is $\tilde{L} = -0.00017$, indicating that the cluster is effectively non-rotating.

Overall, Cluster 1 shows a vortex-like configuration indicative of self-organized, critical motion, while Cluster 2 behaves as a loosely interacting assembly. These contrasting behaviors reflect spontaneous symmetry breaking and a bifurcation in collective dynamics.

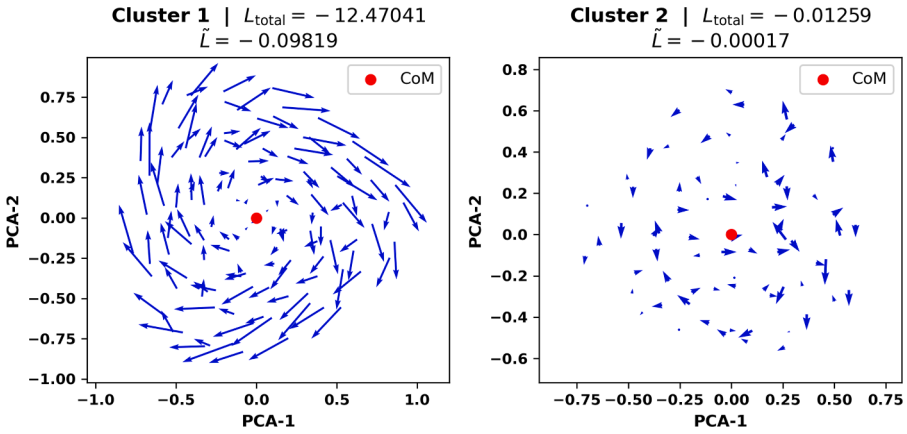

Fig. 9. Velocity vectors and angular momentum in the PCA plane for two clusters. Red dot indicates the CoM.

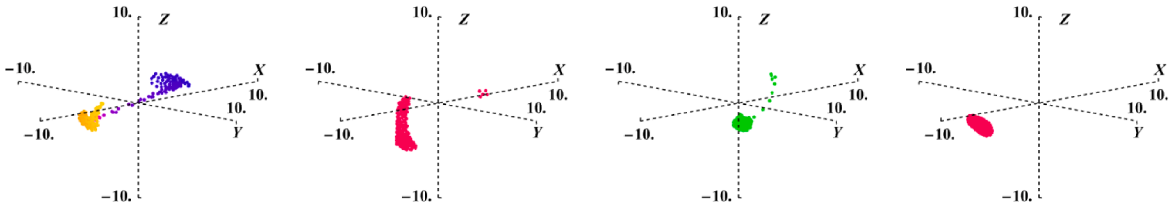

Fig. 10. Swarming in $3D$ space for $b = 0.1$ in the Thomas oscillator at randomly selected time points. Simulations are performed for $N = 200$ over $T = 1500$ time units with $dT = 0.01$ ($J = 0.1$ and $K = 1$), and $\mathcal{V} \approx 3.2$.

For $b = 0.1$, the particles explore a significantly larger spatial volume compared to the previous case. The collective motion leads to a scenario where particles continuously split and recombine, eventually forming a deformable disc-like shape. Occasionally, a few particles deviate from the central disc while maintaining phase coherence. More intriguingly, the system displays behaviour reminiscent of a dense fluid. As b decreases, particle velocities increase, allowing the cluster to explore a broader spatial region. The phase of the cluster oscillates between two fixed values. Fig. 10 illustrates the swarming scenarios at randomly selected time points.

A key observation is that in the chaotic regime of the Thomas oscillator, the cluster exhibits finite displacement, in contrast to the high damping regime where the centre of mass remains stationary. In this dynamic state, the cluster traces a chaotic trajectory through $3D$ space.

3.3. *Swarming states for the conservative regime of the Thomas oscillator [$b = 0$]*

In the absence of damping ($b = 0$), inertial forces dominate, giving rise to large-scale swirling and complex streaming patterns, collectively termed *active turbulence*. The system features an infinite number of unstable fixed points, arranged in a $3D$ grid along three orthogonal directions at $n\pi$, where $n \in \mathbb{Z}$. Swarmalators frequently transition between clusters centred around these points, following circular Zindler-type trajectories. Despite being conservative, the system exhibits chaotic dynamics. Swarmalators continuously move through $3D$ space, undergoing persistent splitting and recombination, which leads to extensive spatial exploration and a large mean square displacement. For large J, phase-cohesive interactions cause swarmalators to form disc-shaped clusters.

To classify these behaviours, we define two states: *Turbulent Synchrony* (TS), where all oscillators share the same phase, and *Turbulent Asynchrony* (TAS), where phases differ but phase-space correlations persist. Both exhibit finite $\mathcal{V}$ and large D. TS typically arises for ($b = 0,\ J > 0,\ K \leq 0$), while TAS is observed for ($b = 0,\ J > 1,\ K = 1$). These states are illustrated in Fig. 11.

The new swarming states are classified based on the mobility of the CoM and particle dynamics. In the first three cases (Table 2), the CoM remains static while particles move ($\mathcal{V} \neq 0,\ D'(t) = \frac{dD}{dt} = 0$). In the latter two, both $\mathcal{V} \neq 0$ and $D'(t) \neq 0$.

Swarming patterns differ notably between $b = 1.2$ and $b = 0$. At $b = 0$, swarmalators form a quivering, unstable disc, resembling an irregular hexagon. Individual swarmalators exhibit low-amplitude, high-frequency chaotic oscillations, confirmed by the power spectrum. Near $b = 0$, the system shows high-amplitude, low-frequency chaos. As b increases from 0 to 1.2, oscillation amplitude decreases while frequency rises, maintaining chaotic dynamics. When the CoM is static, the system forms a complex dissipative structure; when the CoM becomes chaotic, it shifts into a turbulent or active turbulent state.

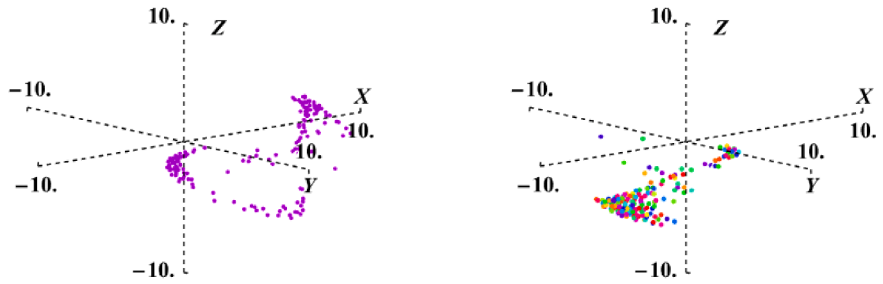

(a) $t = 1300$ (b) $t = 1220$

Fig. 11. Swarming in $3D$ Space for the conservative regime of Thomas oscillator for randomly selected time values. Simulations are done for $N = 200$ for $T = 1500$ time units with $dT = 0.01$ and $b = 0$. (a) TS State for $J = 0.1$ and $K = 1$. (b) TAS state for $J = 0.1$ and $K = -1$.

Table 2
New dynamic swarming states.

#	Asymptotic States	Parameter Values	Abbrevations
1.	Dynamic Sync	$b \gg 0,\ J > 0, K = 1,\ \mathcal{V} \neq 0,\ D'(t) = 0$	DS
2.	Dynamic Async	$b \gg 0,\ J > 0,\ K = -1,\ \mathcal{V} \neq 0,\ D'(t) = 0$	DAS
3.	Phase Asymmetric DCS	$b = 0.5,\ J = 1,\ K = 0^+,\ \mathcal{V} \neq 0,\ D'(t) = 0$	PADCS
4.	Dynamic Cluster Sync	$b = 0.3,\ J = 0.3,\ K = 1,\ \mathcal{V} \neq 0,\ D'(t) = 0$	DCS
5.	Turbulent Sync	$b = 0,\ J > 1,\ K = 1,\ \mathcal{V} \neq 0,\ D'(t) \neq 0$	TS
6.	Turbulent Async	$b = 0,\ J = 1,\ K = -1,\ \mathcal{V} \neq 0,\ D'(t) \neq 0$	TAS

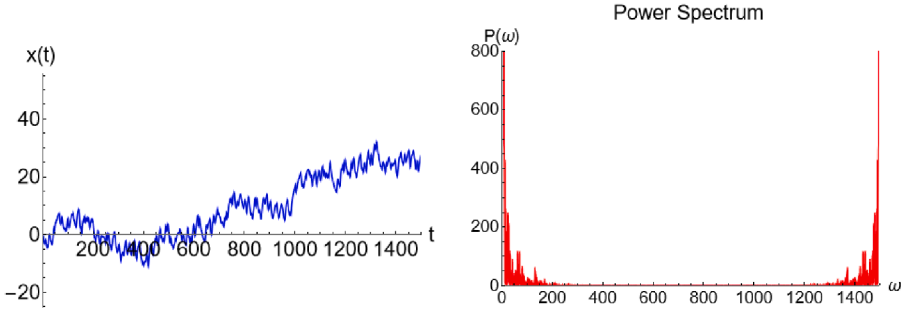

(a) (b)

Fig. 12. **L**eft panel: time series **R**ight panel: power spectra of a randomly selected swarmalator from the circular disc. Simulations are done for $N = 200$ for $T = 1500$ time units with $dT = 0.01$ and $b = 0$. (a,b) $(J,\ K) = (0.1,\ high)$.

Fig. 12 shows that a randomly chosen oscillator exhibits chaotic dynamics, evident from the broadband spectrum spanning both low and high frequencies. This chaotic behavior persists across a wide range of coupling strengths J, though the dominant spectral peaks are more pronounced than in the circular disc configuration.

When the damping parameter is zero, particles move unrestrained, interacting locally and forming feedback loops. These interactions, coupled with minimal damping, amplify small fluctuations into large-scale turbulent patterns resembling fluid vortices. This state, known as *active turbulence*, arises from locally driven, energy-consuming particle motion. The resulting mechanical forces under low damping generate swirling, eddy-like structures. Adaptation through local interactions and environmental influences further induces chaotic self-organization, offering insights into emergent behavior.

The $\mathcal{D}$ vs. b plot (Fig. 13) highlights the link between damping and CoM mobility. At zero damping, an infinite number of unstable fixed points form a $3D$ lattice, allowing extensive phase space exploration. For small J, motion remains chaotic with high mobility. As J increases, swarmalators organize into a circular disc that explores the available space. Higher damping introduces greater dissipation, reducing the number of unstable fixed points and enhancing stability. At high J, the system transitions to one or two stable structures (e.g., circular, Zindler) with diminished mobility. Thus, for a fixed b, J governs the swarm's dynamics, revealing complex phase transitions. The interplay of dissipation and alignment forces drives both mobility and order, shedding light on collective motion in active matter and its practical implications.

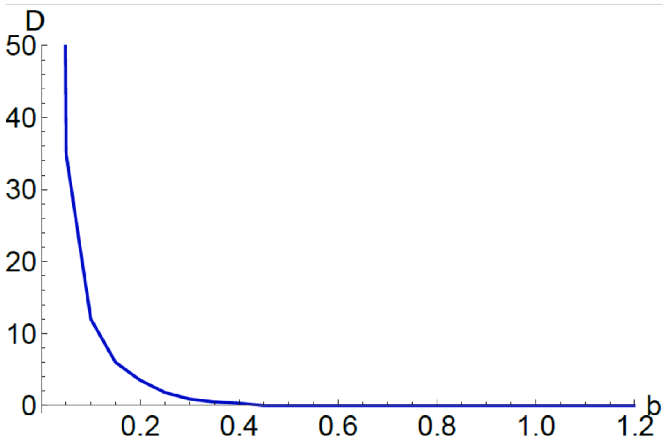

Fig. 13. The D vs b plot. Simulations are done for $J = 0.1,\ K = 1$ and calculated for the asymptotic states using Eq. (6).

4. Results and discussions

The simulation reveals several key observations:

(i) The system self-organizes via feedback loops, adapting to external stimuli.
(ii) Behaviour depends on the environmental interaction parameter b and various coupling strengths among individuals.
(iii) High values of b induce "sticking" behaviour, promoting structural stability.

These are typical of open systems that exchange mass, energy, and information. Fluctuations, amplified by feedback, lead to the formation of stable dissipative structures. The model captures how non-linear interactions and coupling yield emergent patterns and self-organization. The Thomas system models active fluid-like behaviour through swarmalators, whose motion is governed by a damping parameter.

High damping suppresses CoM motion, leading to stable, disc-shaped clusters characteristic of $Non-EquilibriumSteadyStates$ (NESS). Within these clusters, particles exhibit persistent quivering motion, maintaining internal activity despite global stability. The model discussed here includes terms like $J\cos(\Theta_{ij})$, which locally inject energy into the system. Additionally, spatial terms such as $\sin(x)$, $\sin(y)$, and $\sin(z)$ introduce local instabilities, causing particles to undergo oscillatory motion even at high damping values. Thus, the observed behavior is not a contradiction, but a hallmark of driven dissipative systems–typical in active matter. In contrast, low damping permits fluid-like collective movement, resembling active Brownian dynamics, enabling transport and complex self-organization far from equilibrium.

Analogies can be drawn with biological systems: DS states mirror auto-aggregation in genetically similar species, while DAS states reflect co-aggregation of distinct species. APW states resemble stress-induced clustering in fluctuating environments, and TS/TAS states model homogeneous and heterogeneous fluid flow, respectively. Interaction forces shaped by evolution enable survival strategies and energy-efficient transport without a central organiser. Chiral symmetry breaking in swarming systems refers to the spontaneous emergence of handedness—left or right-oriented configurations—from an initially symmetrical setup. It commonly appears in natural swarms (e.g., bacteria, birds, fish), where asymmetric patterns arise despite symmetric conditions. This breaking enables directional motion, structural organization, and adaptive responses, highlighting its key role in development, collective decision-making, and swarm intelligence.

We observed two distinct forms of chiral symmetry breaking. In the first case, both spatial and phase asymmetry emerge as the swarm splits into subgroups with disordered motion and divergent internal rhythms. This suggests functional differentiation, akin to specialization within the swarm. In the second case, despite identical internal phases, the swarm bifurcates spatially into two mirror-image clusters–one forming a vortex-like structure, the other remaining disordered. This spontaneous, leaderless symmetry breaking reflects a system near criticality and highlights mechanisms of emergent complexity relevant to both biological collectives and synthetic swarm robotics.

Zero damping, or the absence of energy-dissipative forces in the system, plays a pivotal role in the swarming model. When $b = 0$, all forms of dissipation are eliminated, enabling particles to move freely in three-dimensional space over time. This results in turbulent, high-energy motion, where particles follow vigorous, coordinated trajectories—including straight lines, loops, and complex paths. The lack of damping allows persistent internal oscillations to be amplified through feedback mechanisms, giving rise to rich spatio-temporal dynamics. Biologically, this behavior mirrors the movement of microorganisms in low-viscosity environments, where propulsion emerges from internal energy absorption and interaction with the surroundings rather than inertial momentum. Strong evidence for active turbulence is the presence of a chaotic power spectrum and significant particle mobility in our system. The broadband nature of the power spectrum indicates spatio-temporal disorder and the excitation of multiple interacting modes, which are characteristic of turbulent-like dynamics. Simultaneously, the high particle mobility reflects enhanced transport and mixing, driven

by fluctuating velocity fields and persistent local flow structures such as vortices. Together, these features point to a nonequilibrium turbulent state—not governed by inertia as in classical turbulence but instead sustained by internal activity at the microscale. This behaviour aligns with the defining signatures of active turbulence observed in various active matter systems. Thus, zero damping is essential for capturing the core characteristics of active, non-equilibrium systems, offering valuable insights into mechanisms of energy-efficient transport and adaptive behavior in both natural and synthetic swarming collectives.

Adaptation is captured through the parameter b: as b increases, swarmalators transition from dynamic, mobile patterns to static yet internally active structures, resembling bacterial swarms adapting to crowded environments. At low b, NESS patterns remain dynamically mobile, while high b leads to globally static but locally active configurations. This reflects how the system reorganizes in response to environmental conditions. Overall, the model reveals mechanisms of self-assembly and adaptation unique to active systems, with implications for self-healing materials, autonomous micro-robots, and behaviors absent in passive matter.

5. Conclusion

The study demonstrates the diverse swarming dynamics governed by the Thomas oscillator with a tunable damping parameter. The system exhibits a wide range of emergent behaviors, highlighting the spontaneous formation of rich and varied swarming states. These transitions are shown to depend sensitively on both the environmental damping and the strengths of inter-agent interactions. Notably, at high damping values, the system forms disc-like, dynamically stable structures, whereas at low damping, it transitions into fluid-like, deformable clusters. These contrasting patterns underscore the system's capacity to model both ordered and fluid swarming regimes, emphasizing the role of damping in shaping collective behavior.

One of the key findings of this study, both novel and intriguing, is the emergence of chiral symmetry breaking in two distinct forms. This phenomenon is connected to group decision-making, subpopulation differentiation, and specialization typically observed in biological swarms. The intermittent coexistence of hexatic and isotropic liquid-like states, without any change in system parameters, highlights the system's proximity to a critical motility threshold—an event particularly relevant to biofilm nucleation. The dynamic switching between order and disorder is a biologically significant observation. Furthermore, the zero-damping scenario captures the turbulent, high-motility behavior characteristic of swarming systems.

Thus, the swarming model captures fundamental aspects of active matter and self-organization, offering valuable insights into adaptive behavior in both natural and synthetic systems. This study opens up promising avenues for applications in robotic swarms, bio-inspired materials, and autonomous decision-making.

CRediT authorship contribution statement

Vinesh Vijayan: Conceptualization, Formal analysis, Investigation; **Pranaya Pratik Das:** Resources, Data curation; **K. Hariprasad:** Project administration, Writing – review & editing; **P. Satishkumar:** Project administration, Writing – review & editing.

Data availability

Data will be made available on request.

Declaration of competing interest

The authors declare that they have no known competing financial interests or personal relationships that could have appeared to influence the work reported in this paper.

During the preparation of this work, the author(s) used `ChatGPT` to enhance language and readability. The content was reviewed and edited accordingly, and the author(s) take full responsibility for its accuracy and integrity.

Acknowledgment

The authors acknowledge that this study is a continuation of the work previously presented work in [27].

Supplementary material

Supplementary material associated with this article can be found, in the online version, at 10.1016/j.cnsns.2025.109216

References

[1] OḰeeffe KP, Hong H, Strogatz SH. Oscillators that sync and swarm. Nat Commun 2017; 8. https://doi.org/10.1038/s41467-017-01190-3
[2] OḰeeffe K, Bettstetter C. A review of swarmalators and their potential in bio-inspired computing. Micro Nanotechnol Sens Syst Appl XI 2019. https://doi.org/10.1117/12.2518682
[3] Igoshin OA, Welch A M RD, Oster D KG. Pattern formation and traveling waves in myxobacteria: theory and modeling. Proc Natl Acad Sci 2001;98:14913–18. https://doi.org/10.1073/pnas.221579598
[4] Ha S-Y, Jung J, Kim J, Park J, Zhang X. Emergent behaviors of the swarmalator model for position-phase aggregation. Math Models Methods Appl Sci 2019;20:2225–69. https://doi.org/10.1142/s0218202519500453

[5] Hong H. Active phase wave in the system of swarmalators with attractive phase coupling. Chaos Interdiscip J Nonlinear Sci 2018;28:103112. https://doi.org/10.1063/1.5039564
[6] Sar GK, Chowdhury SN, Perc M, Ghosh D. Swarmalators under competitive time-varying phase interactions. New J Phys 2022;24:043004. https://doi.org/10.1088/1367-2630/ac5da2
[7] Manna RK, Shklyaev OE, Balazs AC. Chemical pumps and flexible sheets spontaneously form self-regulating oscillators in solution. Proc Natl Acad Sci 2021;118. https://doi.org/10.1073/pnas.2022987118
[8] Aranson IS. Active colloids. Phys Usp 2013;55:79–92. https://doi.org/10.3367/ufne.0183.201301e.0087
[9] Ebbens SJ. Active colloids: progress and challenges towards realising autonomous applications. Curr Opin Colloid Interface Sci 2016;21:14–23. https://doi.org/10.1016/j.cocis.2015.10.003
[10] Patteson AE, Gopinath A, Arratia PE. Active colloids in complex fluids. Curr Opin Colloid Interface Sci 2016;21:86–96. https://doi.org/10.1016/j.cocis.2016.01.001
[11] Zhang J, Luijten E, Grzybowski BA, Granick S. Active colloids with collective mobility status and research opportunities. Chem Soc Rev 2017;46:5551–69. https://doi.org/10.1039/c7cs00461c
[12] Thomas R. Deterministic chaos seen in terms of feedback circuits: analysis, synthesis, “Labyrinth Chaos”. Int J Bifurc Chaos 1999;9:1889–905. https://doi.org/10.1142/S0218127499001383
[13] Thomas R, Kaufman M. Multistationarity, the basis of cell differentiation and memory: I and II. Chaos 2001;11:170–95. https://doi.org/10.1063/1.1350439 https://doi.org/10.1063/1.1349893
[14] Thomas R, Thieffry D, Kaufman M. Dynamical behaviourof biological regulatory networks. I. Biological role of feedback loops and practical use of concept of the loop-charateristics state. Bull Math Bio 1995;57:247–76. https://doi.org/10.1007/BF02460618
[15] Rasmussen S, Knudsen C, Feldberg R, Hindsholm M. The coreworld: emergence and evolution of cooperative structures in a computational chemistry. Phys D Nonlinear Phenom 1990;42:111–34. https://doi.org/10.1016/0167-2789(90)90070-6
[16] Basios V, Antonopoulos CG. Hyperchaos and labyrinth chaos: revisiting Thomas–Rössler systems. J Theor Biol 2019;460:153–9. https://doi.org/10.1016/j.jtbi.2018.10.025
[17] Vijayan V, Ganguli B. Pattern in nonlinearly coupled network of identical Thomas oscillators. Comm Nonlinear Sci Numer Simul 2021;99:105819. https://doi.org/10.1016/j.cnsns.2021.105819
[18] Lisin EA, Vaulina OS, Lisina II, Petrov OF. Active brownian particle in homogeneous media of different viscosities: numerical simulations. Phys Chem Chem Phys 2021;23:16248–57. https://doi.org/10.1039/d1cp02511b
[19] Speck T, Tailleur J, Palacci J. Focus on active colloids and nanoparticles. New J Phys 2020;22:060201. https://doi.org/10.1088/1367-2630/ab90d9
[20] Liebchen B, Löwen H. Which interactions dominate in active colloids? J Chem Phys 2019;150:061102. https://doi.org/10.1063/1.5082284
[21] Wang W, Lv X, Moran JL, Duan S, Zhou C. A practical guide to active colloids: choosing synthetic model systems for soft matter physics research. Soft Matter 2020;16:3846–68. https://doi.org/10.1039/d0sm00222d
[22] Wang Z, Wang Z, Li J, Tian C, Wang Y. Active colloidal molecules assembled via selective and directional bonds. Nat Commun 2020;11. https://doi.org/10.1038/s41467-020-16506-z
[23] Henkes S, Fily Y, Marchetti MC. Active jamming: self-propelled soft particles at high density. Phys Rev E 2011;84(4):040301(R). https://doi.org/10.1103/PhysRevE.84.040301
[24] Jolliffe IT, Cadima J. Principal component analysis: a review and recent developments. Philos Trans R Soc A Math Phys Eng Sci 2016;374(2065):20150202. https://doi.org/10.1098/rsta.2015.0202
[25] Halperin BI, Nelson DR. Theory of two-dimensional melting. Phys Rev Lett 1978;41:121–4.
[26] Nelson DR, Halperin BI. Dislocation-mediated melting in two dimensions. Phys Rev B 1979;19:2457–84.
[27] Vijayan V, Karpagavalli K, Jenifer S, Prakash R. From disorder to design: entropy-driven self-organization in an agent based swarming model and pattern formation. 2025; arXiv preprint arXiv:2503.18401. Submitted March 24, 2025; available at arXiv.